Climate warming has led to the degradation of permafrost stability in the past half century over the Qinghai-Tibet Plateau

Youhua Ran[1,2], Xin Li[1,2,3], Guodong Cheng[1,4]

[1]Key Laboratory of Remote Sensing of Gansu Province, Heihe Remote Sensing Experimental Research Station, Cold and Arid Regions Environmental and Engineering Research Institute, Chinese Academy of Sciences, Lanzhou 730000, China
[2]University of Chinese Academy of Sciences, Beijing 100049, China
[3]CAS Center for Excellence in Tibetan Plateau Earth Sciences, Beijing 100101, China
[4]Institute of Urban Studies, Shanghai Normal University, Shanghai, Shanghai 200234, China

Correspondence to: Xin Li (lixin@lzb.ac.cn)

Abstract. Temperature increases cause a unique type of damage to permafrost. This damage is often expressed as the degradation of permafrost thermal stability, which is very important for engineering design, resource development, and environmental protection in cold regions. This study evaluates the degradation of permafrost stability over the Qinghai-Tibet Plateau (QTP) from the 1960s to the 2000s using estimated decadal mean annual air temperatures (MAATs) by integrating remote sensing-based estimates of mean annual land surface temperatures (MASTs), leaf area index (LAI) and fractional snow cover values, and decadal mean MAATs taken at 152 weather stations using geographically weighted regression (GWR). The results reflect a continuous rise of approximately 0.04 ℃/a in the decadal mean MAAT values over the past half century. Climate warming has led to a reduction in permafrost stability in the past half century. The total degraded area of stability is approximately 153.76×10^4 km^2, which corresponds to 87.98% of the permafrost area in the 1960s. The stability of 75.24% of the extremely stable permafrost, 89.56% of the stable permafrost, 90.3% of the sub-stable permafrost, 92.31% of the transitional permafrost, and 32.8% of the unstable permafrost has been reduced to lower levels of stability. Approximately 49.4% of the unstable permafrost and 95.95% of the extremely unstable permafrost has degraded to seasonally frozen ground. The sensitivity of the permafrost to climate is dependent on its stability level. The mean elevations of the extremely stable, stable, sub-stable, transitional, unstable, and extremely unstable permafrost areas increased by 88 m, 97 m, 155 m, 185 m, 161 m and 250 m, respectively. The degradation mainly occurred from the 1960s to the 1970s and from the 1990s to the 2000s. This degradation has led to increases in risks to infrastructure, increased flood risks, reductions in ecosystem resilience, and positive climate feedback effects. It therefore affects the well-being of millions of people and sustainable development at the Third Pole.

1 Introduction

Permafrost is defined as earth materials that include ice or organic material and remains at or below 0 ℃ for at least two years (Permafrost Subcommittee, National Research Council of Canada. 1988; Williams et al., 1989). Temperature rise

causes a unique type of dynamic damage to permafrost (Zhu et al., 2016). This damage is often expressed as the degradation of permafrost thermal stability, which is very important for engineering design, construction, resource development, the carbon and water cycles, and ecological protection in cold regions (Collett, 2002; Cheng and Wu, 2007; Tarnocai et al, 2009; Schuur et al, 2009; Schaefer et al, 2011; Hinzman et al., 2013; Mu et al., 2015). In terms of middle- and high-elevation permafrost regions, the area of permafrost in the Qinghai-Tibet Plateau (QTP) is the largest in the world. The permafrost in the QTP experiences higher temperatures than those observed in Siberia and the Arctic, which are more sensitive to global climate warming and human activity (Wu et al., 2002; Haeberli and Hohmann, 2008; Li et al., 2008; Ran et al., 2012; Ran and Li, 2016).

Monitoring and simulation show that substantial permafrost degradation is occurring on the QTP. For example, the mean annual air temperature (MAAT) increased by approximately 0.2~0.4 ℃ from the 1970s to the late 1990s (Wang et al., 2000). From 1961–2010, the decadal average MAAT rose by 1.3 ℃, with an average rate of increase of 0.03 ℃/a (Jin et al., 2011; Ran and Li, 2016). From 1996 to 2001, the thickness of the active layer increased by 0.15~0.50 metres, and the mean annual ground temperature (MAGT) rose by 0.1–0.5 ℃ in the past 30 years (Yang et al., 2010). At Xidatan, which is near the city of Golmud and at the northern boundary of the permafrost on the QTP along the Qinghai-Tibet Railway (QTR), the lower limit of permafrost (the lowest elevation of permafrost occurrence) moved upward by approximately 25 m from 1975 through 2002 (Nan et al., 2003). The lower limit of permafrost on the northern and southern slopes of the Bayan Har Mountains, where a region of discontinuous permafrost occurs in the southern part of Qinghai Province, moved upward by approximately 100 metres and 90 metres, respectively, from 1991 to 2010 (Luo et al., 2012). During 2006 to 2012, on the southern side of the Tanggula Mountains permafrost region along the QTR, both the engineered structures and ongoing climate change caused the permafrost degradation to accelerate. For the areas of undisturbed permafrost and permafrost under an embankment, the active layer deepened by 0.29 m and 0.41 m, and the ground temperature at a depth of 10 m rose by 0.03 ℃ and 0.06 ℃, respectively (Sun et al., 2014). Cheng et al. (2012) reported on the decadal changes in permafrost distribution on the QTP over the past 50 years (1960–2009) and demonstrated that the rate of permafrost loss had accelerated since the 1980s, and about one-fifth of the total area of permafrost that existed in the 1960s has degraded.

However, many of these studies focus on either the local or in situ scales, and few studies have focused on the regional scale. Although the decadal changes in the permafrost distribution over the QTP were simulated by Cheng et al. (2012), this study emphasized the migration of permafrost “boundaries” based on the relation between air temperature and the lower limit of the permafrost. Naturally, these boundaries are continuous, inexact representations of the permafrost distribution and permafrost degradation (Yang et al., 2010). Ran and Li (2016) assessed the degradation of permafrost stability in China over the past 30 years; however, this study used a near-surface air temperature reanalysis dataset with low resolution and large uncertainties. These studies are not comprehensive and do not adequately reflect changes in the thermal state of the permafrost, especially in the interior of permafrost zones and at high spatial resolution. Additionally, regional-scale evaluations usually rely on meteorological data. The most commonly used variable is air temperature, but measurements of this quantity are sparse on the QTP. Although the sparse air temperature measurements are interpolated onto grids based on digital elevation models (DEMs),

the uncertainty of the gridded air temperatures is significant because of the heterogeneity of the surface characteristics, including snow cover and vegetation, and the locations of weather stations (Vancutsem et al., 2010). Fortunately, the remote sensing era has led to changes in this situation. Thermal infrared remote sensing provides direct observations of land surface temperatures (LSTs) at high spatial and temporal resolutions. For example, the Moderate Resolution Imaging Spectroradiometer (MODIS) LST product is freely available and has been validated over large areas via a series of field campaigns. Its accuracy is better than 1 ℃ (0.5 ℃ in most cases) (Wan et al, 2002; 2004; 2008). Remote sensing-based estimates of LSTs provide a key high-resolution temperature pattern of the land surface that can potentially be used in monitoring degradation; however, criteria for using LST estimates to distinguish permafrost types are not traditionally available, and the relatively short time series of LST data does not meet the needs of long-term permafrost monitoring. Of the three commonly used predictors for permafrost, the MAGT and permafrost thickness are the most direct indicators of the thermal stability of permafrost (Cheng, 1984); however, long-term measurements of the MAGT and permafrost thickness are almost impossible due to the high cost of drilling boreholes. The MAAT is frequently used in mapping the distribution of permafrost. It is easy to measure and has high spatial representativeness. Importantly, long-term in situ measurements of MAATs are available, and it is possible to estimate MAATs over the QTP using remote sensing-based methods. Therefore, the remote sensing-based LST values can be converted to MAATs and used to monitor the permafrost thermal state, although the potential problems of the MAAT model in predicting permafrost degradation are well known. For example, the performance of the MAAT model is generally affected by the thermal inertia of deep soil layers and geothermal flux (Smith and Riseborough, 2002; Jin et al., 2006; Wu et al., 2010a).

Several previous studies have demonstrated the potential of satellite-based methods in estimating near-surface air temperatures (Hachem et al., 2009; 2012; Vancutsem et al., 2010; Yao and Zhang, 2013). The variation in the uncertainty is mainly related to the underlying surface type such as snow cover and vegetation, the amount of solar radiation, and cloud cover (Henderson-Sellers and Hughes, 1982; Zhang, 2005; Vancutsem et al., 2010; Lawrence et al., 2011; Hachem et al., 2012; Ran et al., 2015). Additionally, the highly accurate remote sensing-based snow cover and vegetation products are also available. All of these remote sensing-based data products are very important for estimating the MAAT, which is an air temperature index used in monitoring the thermal stability of permafrost.

Therefore, the objective of this study is to evaluate the degradation of permafrost stability over the QTP from 1960 to 2010 by integrating multi-criterion remote sensing observations and an air temperature observation network.

2 Methods and Datasets

In this study, the degradation of permafrost stability is evaluated based on the MAAT model and the improved MAAT data over the QTP in the past half century. The MAAT in situ measurement data at 152 sites over the QTP and remote sensing data with six independent variables were combined using a Geographically Weighted Regression (GWR) model to estimate the MAAT with a 1 km resolution over the QTP during the past five decades.

2.1 Permafrost thermal stability classification system

We use the thermal stability permafrost classification system proposed by Cheng (1984). In this system, permafrost is classified into extremely stable, stable, sub-stable, transitional, unstable, and extremely unstable types, as shown in Table 1. This system is more useful to describe permafrost degradation from an engineering perspective, rather than changes in the extent of permafrost. The MAAT criterion is available in this system to assess the stability types. On the QTP, a MAAT of −2 ℃ has typically been used to distinguish permafrost from seasonally frozen ground (Cheng, 1984; Ran and Li, 2016). The permafrost stability system was proposed based on the MAGT measurement as an index by analysis of the three-dimensional zonation of the high-elevation permafrost (vertical, latitudinal, and aridity). It is a high level summary of high altitude permafrost zonation. The MAAT index was given according to the statistical relation between MAGT, elevation, and the in situ MAAT measurement (Cheng, 1984). However, the extremely unstable type in the thermal stability classification system proposed by Cheng (1984) refers to regions that include cave ice and frozen gravel below the lower limit of permafrost, which is a very scattered distribution. In this paper, a MAAT of −1 ℃ is simply used to distinguish extremely unstable permafrost from seasonally frozen ground.

2.2 Simulation of MAAT using geographically weighted regression

In this study, geographically weighted regression (GWR) is used to simulate MAATs. Local parameters are employed in the GWR model to estimate MAATs while considering the spatial locations of meteorological stations (Brunsdon et al., 1998; Kumar et al., 2012). The weighting is a function of the distance between the location of each regression point and the sites where observations are available. The GWR model used in the present study is shown below in Equation (1):

$$y_i = \beta_0(\mu_i, \upsilon_i) + \sum_{k=1}^{m} \beta_k(\mu_i, \upsilon_i) x_{ik} + \varepsilon_i \quad (1)$$

where y_i is the MAAT at pixel i, x_{ik} is the k[th] explanatory factor at pixel i, $\beta_0(\mu_i, \upsilon_i)$ and $\beta_k(\mu_i, \upsilon_i)$ represent the intercept and slope for the k[th] explanatory factor, m is the number of explanatory factors, and ε_i is the residual term. The quantities $\beta_0(\mu_i, \upsilon_i)$ and $\beta_k(\mu_i, \upsilon_i)$ are estimated using Equation (2):

$$\hat{\beta}(\mu_i, \upsilon_i) = (X^T W(\mu_i, \upsilon_i) X)^{-1} X^T W(\mu_i, \upsilon_i) Y \quad (2)$$

where $\hat{\beta}(\mu_i, \upsilon_i)$ is an unbiased estimation of the regression coefficients. It is a vector that includes an intercept and *m* regression coefficients associated with *m* explanatory factors, i.e., the 6 independent variables selected by a stepwise linear regression analysis (see below). X is a matrix of explanatory factors ($n \times m$); $W(\mu_i, \upsilon_i)$ is the spatial weight matrix,

which is a diagonal matrix; Y is a vector ($n \times 1$) for the dependent variables, i.e., the decadal mean MAAT in the 1960s, 1970s, 1980s, 1990s, and 2000s; and n is the number of MAAT observation stations for each year.

In this study, the Gaussian function is used as a spatial weighting function, as shown in Equation (3):

$$W(\mu_i, \upsilon_i) = \exp(-\frac{1}{2}(\frac{d_i}{r})^2) \quad (3)$$

where d_i is the distance between the *i*th observation station and the point to be estimated, and r is the bandwidth parameter. To accommodate different station densities, the corrected Akaike information criterion (AICc) is used to determine the optimal bandwidth parameters.

A stepwise linear regression analysis is used to select the independent variables for the GWR model (Table 2). The analysis shows that the use of the MAST, the leaf area index (LAI), the fractional snow cover (FSC), elevation, latitude, and longitude as independent variables results in the highest degree of explanatory power for the past five decades, and the significance level is less than 0.0001. The variance inflation factor (VIF) is used to assess the multicollinearity of the model. A VIF value <1.5 shows that the degree of tolerance is high, and the multicollinearity of the model is thus acceptable. The performance of the GWR model in the 2010s is shown in Table 2. The five GWR models are then used to estimate the decadal mean MAAT over the QTP for the past five decades. The SAGA (System for Automated Geoscientific Analyses) (Conrad et al., 2015) is used to implement the GWR. Specifically, the GWR for multiple predictor grids geoprocessing tool is used. The Gaussian weighting function and the global search range are used.

Due to the unavailability of the vegetation, snow cover, and LST datasets during the 1960s to 2000s, the effect of the dynamics of vegetation, snow cover, and LST on MAAT during this period is unknown. This will inevitably cause some errors in the estimation of MAAT. Recent studies show that vegetation is increasing overall during the past 30 years, and the snow cover is decreasing overall during the past 15 years over the QTP (Wang et al., 2016; Huang et al., 2017). The effect of vegetation and snow cover change on MAAT and its feedback process is highly complex. For example, the vegetation-snow interaction effect on MAAT is related to humidity (Zhong et al., 2010; Wang et al., 2013; Wu et al., 2015; Yuan et al., 2017). However, we believe this error mainly occurs at the local level in the nature vegetation dominated areas where the change has occurred at the local level within the last 50 years (Wang et al., 2016; Huang et al., 2017), and it can be partially compensated by the in situ MAAT measurement over the QTP for the past 50 years.

2.3 Evaluation of the degradation of permafrost thermal stability

The following linear regression model is used to evaluate the warming rate or degradation rate over the QTP in the past 50 years:

$$Y = a + bx + \varepsilon \quad (4)$$

where Y denotes the MAAT or permafrost area, x is the time, ε is the error, a is the intercept, and b is the slope (i.e., the warming rate or degradation rate). The statistical significance of the warming rate or degradation rate is evaluated using Student's *t*-test.

Thirteen elevation ranges (<3600 m, 3600-3800 m, 3800-4000 m, 4000-4200 m, 4200-4400 m, 4400-4600 m, 4600-4800 m, 4800-5000 m, 5000-5200 m, 5200-5400 m, 5400-5600 m, 5600-5800 m, and >5800 m) are used to evaluate the elevation dependence of the warming rate. The degradation of permafrost thermal stability is evaluated from two perspectives, the change in area of the different thermal stability types and the spatial heterogeneity of the change. For the area change, we calculate the total area of each thermal stability type during the past five decades and the rate of change (i.e., the degradation rate) using the linear regression model shown in Equation (4). The spatial pattern of the degradation of permafrost thermal stability is evaluated at two levels. At the pixel level, the spatial distribution of the degradation is evaluated. At the level of the thermal stability types, a transfer matrix is used to evaluate the conversions among the thermal stability types (Stehman, 1997). We also analyse the changes in the elevation histograms for each thermal stability type in the past 50 years.

2.4 Datasets

2.4.1 Mean annual land surface temperature

MODIS Terra/Aqua daytime and nighttime LST products (MOD11A1 and MYD11A1, version 5) with a spatial resolution of 1 km and covering 2006 to 2010 were acquired from the Distributed Active Archive Center (DAAC) operated by the U.S. National Aeronautics and Space Administration (NASA). These data are used in this study to estimate MASTs. A pragmatic approach proposed by Ran et al. (2015; 2017) is employed to estimate the MASTs using the four daily MODIS LST products. This approach assumes that the arithmetic average of the daytime and nighttime LSTs represent the daily mean LST with acceptable accuracy, and the daily amplitude of LST is more homogeneous than the LST itself (Liu et al., 2006; Kogan et al., 2011; Ran et al., 2015). The approach allows the full use of every value at any time in any pixel of the MODIS LST products through the use of the temporally and spatially complete LST daily amplitude, which is interpolated using a gap filling algorithm (Garcia, 2010). This algorithm employs a penalized least squares regression based on discrete cosine transforms that explicitly utilize information from a time series to predict the missing values. The penalized least squares regression is a thin-plate spline smoother for a generally one-dimensional data array, and it can trade off fidelity to the data versus the roughness of the mean function (Garcia, 2010; Wang, et al., 2012). This approach is easy to implement and independent of other observations. Validation shows that the scheme is effective in restoring the missing values in MODIS instantaneous LST observations and produces a spatially and temporally continuous daily average LST dataset that displays good agreement with observations made at the ground

surface. The errors in the results originate mainly from the original instantaneous LST MODIS products. A more detailed description of this scheme can be found in Ran et al. (2015; 2017). The temporally and spatially continuous daily mean LSTs from January 1, 2006 to December 31, 2010 and the corresponding MASTs used in this study are produced using the above approach.

2.4.2 Fractional snow cover

Arithmetic mean values of daily cloud-removed FSC products from 2006 to 2010 are used in this study. This product is derived from the daily MODIS 500-m snow cover product (MOD10A1) using a gap filling process based on a cubic spline interpolation algorithm. A comparison with reference FSC data obtained from Landsat Enhanced Thematic Mapper Plus (ETM+) shows the high accuracy with which this product reflects snow cover information over the QTP (Tang et al., 2013). The cloud-removed FSC products were acquired from the Cold and Arid Regions Science Data Center in Lanzhou, China (http://westdc.westgis.ac.cn).

2.4.3 Leaf area index

Annual mean LAI values obtained from the Global Land Surface Satellite (GLASS), which make up a high-quality LAI product with an eight-day temporal resolution and a 1-km spatial resolution and cover the period from 2006 to 2010, are used in this study. The GLASS LAI product is derived from the fused MODIS and CYCLOPES LAI products, and the remaining effects of cloud contamination have been removed using MODIS time series surface reflectance data and general regression neural networks (Xiao et al., 2014). The results of validation show that the GLASS LAI product has a lower uncertainty than the MODIS and CYCLOPES LAI products (Xiang et al., 2014). The GLASS LAI product was acquired from the GLASS project website (http://glass-product.bnu.edu.cn/en).

2.4.4 In situ MAAT observations

The MAAT measurements, which were collected at 131 stations for the 1960s and 1970s, 133 stations for the 1980s, 144 stations for the 1990s, and 152 stations for the 2000s within the QTP and the surrounding area, were acquired from the data centre of the China Meteorological Administration (http://cdc.nmic.cn). The distribution of the 152 stations for the 2000s is shown in Figure 1. The density of stations in the eastern QTP is higher than other years. The decadal mean MAAT values over the past five decades are used in this study.

2.4.5 Validation data

Validation of the long-term stability of permafrost is difficult due to the limited amounts of reference data that are available. In this study, we evaluate the results by comparing the estimated permafrost distribution in the 2000s with previous regional-scale permafrost maps and borehole measurements at individual sites. The permafrost maps that cover the QTP from

Li and Cheng, (1996), Nan et al. (2002), and Zou et al., (2016) are used at the regional scale. In particular, the map of Zou et al., (2016) integrates the MODIS eight-day LST product within the framework of the temperature at the top of the permafrost (TTOP) model (Smith and Riseborough, 1996), and careful validation of this map has been performed using MAGT data. At the site scale, the MAGT values used in this study were collected from 142 boreholes presented in the existing literature (Yu et al., 2008; Wang et al., 2013; Luo et al., 2013) and the International Permafrost Association (IPA)-International Polar Year (IPY) Thermal State of Permafrost (TSP) Snapshot Borehole Inventory downloaded from the National Snow and Ice Data Center (NSIDC) (http://nsidc.org) (International Permafrost Association, 2010). The distribution of these boreholes is shown in Figure 1.

2.4.6 Ancillary data

The distribution of water bodies in the MODIS land cover product (MOD12Q1) and the map showing the distribution of glacier ice from the second Chinese glacier inventory are used to support the permafrost area statistics. The MOD12Q1 product is used for consistency with the other remote sensing products employed in this study. On the other hand, the glacier extents from the second Chinese glacier inventory are compiled based on Landsat TM/ETM+ images acquired from 2004 to 2011, as well as other ancillary data, such as digital elevation models (DEMs). The robust band ratio segmentation method is first used to delineate the glacier outlines, and intensive manual improvements are then performed to improve its accuracy. An error assessment shows that the area error for all of the glaciers in China is approximately 3.2% (Guo et al., 2015).

3 Results

Decadal mean MAAT estimates with a resolution of 1 km over the QTP in the past 50 years are produced using the GWR model. The mean coefficient of determination of this model is approximately 0.95. The permafrost stability map in the past five decades is then produced based on the simulated MAAT and the permafrost stability types defined in Table 1.

3.1 Change of MAAT over the QTP in the past 50 years

The MAATs over the QTP have risen continuously in the past 50 years. The mean MAAT values for the 1960s, 1970s, 1980s, 1990s, and 2000s are -2.38 ℃, -1.85 ℃, -1.78 ℃, -1.32 ℃, and -0.58 ℃, respectively. These values reflect a continuous rise with a rate of approximately 0.04 ℃/a. This value is higher than the global average warming rate, as well as the estimated warming rates for the QTP reported by Cheng et al. (2012) and Ran et al. (2016) that are based on interpolated elevation-based air temperature data or surface air temperature reanalysis data. The warming rate in the western part of the QTP is higher than that in the eastern part and depends on elevation, as shown in Figures 2 and 3. The warming rate increases with increasing elevation from approximately 0.33 ℃ per decade at 3600 m to 0.49 ℃ per decade at 5200 m. This finding is similar to that of previous studies (Liu and Chen, 2000; Qin et al., 2009). The physical mechanisms of this phenomenon may

be related to the combined effects of the cloud-radiation and snow-albedo feedbacks (Giorgi et al., 1997; Liu et al., 2009; Pepin et al., 2015). These elevated warming rates may have a substantial impact on the thermal stability of the permafrost.

3.2 Thermal stability degradation

Based on the map of permafrost stability types covering the past five decades (Figure 4a-e), we analyse the degradation from three perspectives, including temporal changes, spatial changes in the map plane, and spatial changes with elevation.

3.2.1 Temporal dynamics of thermal stability

The permafrost thermal stability has degraded continuously over the past 50 years. The area occupied by the stable types has decreased continuously, and the area occupied by the unstable types has increased continuously (Table 3). The areas occupied by the extremely stable, stable, sub-stable, and transitional types display net decreases of approximately 8.99×10^4 km^2 (72.79%), 27.06×10^4 km^2 (70.12%), 9.30×10^4 km^2 (27.24%), and 1.18×10^4 km^2 (4.77%) from the 1960s to the 2000s, respectively. In particular, the stable type displays the most serious degradation, and its rate of loss is approximately 6.15×10^4 km^2 (15.94%) per decade. Moreover, the area occupied by the unstable type has increased by approximately 3.99×10^4 km^2 (9.02%) at a rate of 1.06×10^4 km^2 (2.4%) per decade. Specifically, this degradation mainly occurred during the 1960s to 1970s and the 1980s to 1990s for the extremely stable type, the 1960s to the 1970s and the 1990s to the 2000s for the stable type, and the 1980s to the 2000s for the sub-stable type. The area occupied by the extremely unstable type has not changed substantially. Overall, the warming climate has caused a degradation of permafrost stability. If glaciers and the extremely unstable type are included, the total permafrost area has decreased significantly from 174.76×10^4 km^2 in the 1960s to 133.1×10^4 km^2 in the 2000s at a rate of approximately 9.52×10^4 km^2 (5.45%) per decade, and this loss of area occurred mainly during the 1960s to the 1970s and the 1990s to the 2000s (Table 3).

3.2.2 Spatial changes in thermal stability

The degradation of thermal stability has occurred over a broad region of permafrost on the QTP within the past 50 years, especially during the 1960s to the 1970s and the 1990s to the 2000s. The degradation of permafrost stability in the western QTP was serious during the 1960s to the 1970s. In the subsequent 40 years, the degradation of permafrost stability in the QTP was relatively homogeneous (Figure 4f-i). Specifically, the extents of the extremely stable, stable, and sub-stable types retreated from the south to the north (Figure 4a-e). The extents of the transitional, unstable, and extremely unstable types extended northward correspondingly. Approximately 42.30% of the area occupied by the extremely stable type, 42.09% of the area occupied by the stable type, and 39.83% of the area occupied by the sub-stable type have degraded to the stable, sub-stable, and transitional types from the 1960s to the 1970s, respectively. At the same time, approximately 57.26% of the area occupied by the transitional type, 29.34% of the area occupied by the unstable type, and 59.47% of the area occupied by the extremely unstable type, have degraded to the unstable type, the extremely unstable type, and seasonally frozen ground,

respectively. Overall, approximately 75.24% of the area occupied by the extremely stable type, 89.56% of the area occupied by the stable type, 90.3% of the area occupied by the sub-stable type, 92.31% of the area occupied by the transitional type, and 32.8% of the area occupied by the unstable type have degraded to lower levels of stability in the past 50 years (Table 4). The reduction in the area occupied by the permafrost is mainly due to the degradation of the area occupied by the unstable and extremely unstable types. Approximately 49.4% of the area occupied by the unstable type and 95.95% of the area occupied by the extremely unstable type has degraded to seasonally frozen ground (Table 4). The total degraded area is approximately 153.76×10^4 km^2, which accounts for 87.98% of the area occupied by the permafrost region in the 1960s (Figure 4j). The area of permafrost for which the stability has not changed is approximately 21×10^4 km^2 (12.02%). This area is mainly distributed in the central part of the plateau, which contains extremely high mountains, and it is dominated by the extremely stable type. Notably, the stability of a permafrost area of approximately 1.63×10^4 km^2 has increased. This area is found primarily east of Lhasa in the southeastern part of the QTP, which is a major centre of marine glaciers and snow cover in China (Figure 4j). The increased permafrost stability in this area may have large uncertainties; the uncertain MAAT trend is estimated using regression parameters that are appropriate for low-elevation areas, due to the lack of long-term MAAT measurements in the high mountain regions where glaciers and snow are prevalent. The effects of snow or glacier cover may be more important than those of the MAAT. Although records of long-term snow cover and glacier changes in the past 50 years are not available in this study, the sensitivity of glacier and snow cover in a warming climate is dependent on the climate zone. Low snow–climate sensitivities have been found in continental interior climates with relatively cold and dry winters (Brown and Mote, 2009). Larger glaciers have lower climate sensitivities (Ding and Haeberli, 1996; Ye et al., 2001).

Additionally, the complex process and limited knowledge for permafrost-glacier interactions may enhance the uncertainty (Haeberli, 2005; Otto and Keuschnig, 2014). Therefore, we believe the permafrost stability in this area has not changed substantially in the past 50 years, based on this low climate sensitivity.

3.2.3 Elevation changes in permafrost stability type distributions

The elevation statistics of the distribution of the permafrost stability types over the QTP in the past five decades indicate that the elevation occupied by each permafrost stability type in the QTP has increased continuously (Table 5). For the extremely stable type, the mean elevation of the distribution decreased from 5240 m to 5161 m from the 1960s to the 1970s and then rose continuously at a rate of approximately 56.4 m per decade. The reduction in elevation is mainly due to the degradation of the extremely stable permafrost type in the Kailas Mountains. This caused the fluctuation of the mean elevation for extremely stable permafrost during the 1970s to 1980s and reduced its statistical significance (low R in Table 5) for the increasing rate of mean elevation over the past 50 years. Overall, in the past 50 years, the mean rate of increase of the extremely stable type has been approximately 24.7 m per decade. Moreover, the mean elevation of the stable, sub-stable, transitional, unstable, and extremely unstable types have risen at a rate of 23.6 m, 36.3 m, 43 m, 36.5 m, and 56.2 m, respectively. Overall, the mean elevation of the extremely stable, stable, sub-stable, transitional, unstable, and extremely unstable types increased by 88 m, 97 m, 155 m, 185 m, 161 m, and 250 m, respectively, over the past 50 years. This result

indicates that the climate sensitivity of permafrost is dependent on the stability level. The extremely unstable permafrost type is the most sensitive of the permafrost types to climate warming. As in the last section, the degradation mainly occurred from the 1960s to the 1970s and from the 1990s to the 2000s.

4 Discussion

4.1 Cross validation and uncertainty analysis

We validate the permafrost extent only in the 2000s because long-term records of permafrost stability and extent are not available in earlier periods, as mentioned in section 2.4.5. Comparison of the estimated permafrost extent in the 2000s with the permafrost map provided by Zou et al., (2016) shows that the difference is small. Within permafrost areas, the extremely unstable type of permafrost mainly refers to cave ice and frozen gravel, which are distributed below the lower limit of permafrost (Cheng, 1984). This kind of permafrost is usually not counted in the total area of permafrost. Therefore, the permafrost area in the 2000s is approximately $107.19 \times 10^4\ km^2$ if glaciers and lakes are neglected. This result is similar to that of Zou et al., (2016), who showed that the permafrost area in the 2000s was approximately $106.47 \times 10^4\ km^2$. The permafrost distribution is also very similar to that presented by Zou et al., (2016) (Figure 5b). The consistency between the two distributions is 92%, and the kappa coefficient is approximately 0.82. At the site scale, 89% of the 142 locations are consistent with the borehole survey, whereas this proportion is only 74%, 28%, and 86% for the maps of Li and Cheng, (1996), Nan et al. (2002), and Zou et al. (2016), respectively. These proportions indicate that the accuracy of the permafrost extent identified in this study is at least comparable with that of Zou et al. (2016).

The uncertainty of the results may result primarily from the MAAT model, insufficient resolution, inaccuracies in the surface station data, or the sparseness of these stations, which are especially sparse in high mountain areas. First, the response time and the depth to which permafrost is affected by climate warming depend on the extents, durations, amplitudes, and rates of climate warming and are closely related to soil types, surface coverage, ice content, groundwater occurrence, geothermal anomalies, and human activities (Stieglitz et al., 2003; Zhang, 2005; Lawrence et al., 2008; Cheng and Jin, 2013; Westermann et al., 2016). For example, the low heat conductivity of soil leads to lags between increases in surface temperatures and the subsequent increases in permafrost temperature or reductions in permafrost thickness (Li et al., 1996). The delay time is longer for permafrost thickness than temperature and varies with the thermal stability type (Li et al., 1996; Wu et al., 2010a). For the stable type, the degradation of permafrost may be delayed by “thermal offset” and “seasonal offset” effects in the permafrost table due to the negative heat budget; i.e., the amount of heat released from the active layer during the winter is greater than the amount of heat absorbed in summer (Smith and Riseborough, 2002; Wu et al., 2010a). For the unstable type, a positive heat budget appears in the upper soil layer that leads to a greater degradation rate than that seen in stable permafrost, since the thickness of the unstable type is smaller than that of the stable type (Li et al., 1996; Wu et al., 2010a). However, the complex physical mechanisms of the interactions between climate change and permafrost are currently poorly understood (Jin et al., 2011), and a large degree of uncertainty may exist in previous evaluations as well as the permafrost area change over

the past 50 years in this study. Despite current warming, large permafrost areas may persist due to the thermal inertia of permafrost (Cheng et al., 2012). Second, the thawing of the base of the permafrost induced by the geothermal heat flux leads to the permafrost degrading from bottom to top (Jin et al., 2006; Wu et al., 2010a). The MAAT model cannot reflect the change of geothermal flux from the crustal interior. Additionally, the geothermal flux data are generally limited or unavailable. The missing geothermal heat flux may lead to a delay in permafrost degradation, especially for the stable permafrost, because the geothermal flux is independent of air temperature. Third, although the resolution of the simulation has been significantly improved to 1 km, it is still coarse relative to the degradation rate of mountain permafrost. The degradation of mountain permafrost is presented in terms of the increase in the elevation of the lower limit of the permafrost, which is generally approximately a hundred metres. A 1 km change in the horizontal extent change may correspond to a change in elevation of hundreds of metres. Last, the lack of long-term MAAT measurements in the glacier- and snow-dominated high mountain regions may lead to errors in the estimated MAATs.

Overall, the "accelerated degradation" effect of the MAAT model may be partly counteracted by the "delayed degradation" effect of the missed geothermal heat flux. Long-term observation shows that the mean increasing rate of ground temperature at 10-20 m depth in the QTP is approximately 0.024 ℃ (Zhao et al., 2010; Wu et al., 2010b; Jin et al., 2011), which is comparable with the warming rate of air temperature. This shows that the evaluation results of permafrost stability degradation using the MAAT model is generally accepted at the overall QTP scale.

4.2 The implications of the degradation of thermal stability

The degradation of permafrost stability in the QTP has important impacts on the safety of infrastructure in permafrost regions, water quality, ecosystem health, and the feedbacks on regional and global climates. First, as the permafrost stability degrades, the risk of deterioration and damage to engineered structures in permafrost zones will increase. This indicates that the measures used to prevent permafrost degradation may need to be enhanced for new structures. For example, permafrost accounted for 90.1% of a 10-km-long segment of the QTR from Golmud to Lhasa in the 1960s, and these permafrost areas were dominated by the sub-stable type; however, after 50 years (i.e., in the 2000s), these permafrost areas accounted for only 67.77% and were dominated by the unstable type. For "warm" permafrost areas that are dominated by unstable permafrost, an enhanced measure to prevent permafrost degradation, i.e., the proactive roadbed cooling approach, has been successfully applied in constructing the QTR (Cheng, 2004; 2005; Cheng et al., 2008). Second, the degradation of permafrost in the QTP may affect the hydrologic cycle in the Third Pole region, which includes the QTP and the surrounding arid regions. Permafrost controls the distribution, recharge, flow paths, discharge, dynamics, and hydrochemistry of groundwater (Cheng and Jin, 2013). The degradation of permafrost affects the interactions among the surface water, subsoil water, and groundwater by changing the hydraulic conductivity and hydraulic connectivity of the soil. The degradation of the ice-rich permafrost itself makes important contributions to surface runoff and the development of thermokarst lakes in the inner Tibetan Plateau (Zhang et al., 2013). The enhanced drainage may lead to increases in flood risk (Larsen et al., 2008) and reductions in ecosystem resilience via seasonal shifts in stream flow and groundwater abundance, because the decrease in

permafrost water storage capacity in the QTP will lead to a reduction in dry-season water availability. All of these changes will affect the well-being of millions of people and sustainable development at the Third Pole, which contains the headwater areas of several of the major rivers in Southeast Asia, such as the Yellow, Yangtze, Mekong, Yarlung Zangbo and Shiquan Rivers. The Third Pole also includes many inland rivers, such as the Shiyang, Heihe, Shule, and Tarim Rivers, in northwestern China. Last, the permafrost region in the QTP contains approximately 160 Pg of organic carbon (Mu et al., 2015) and many thermokarst lakes and wetlands (Niu et al., 2011; Luo et al., 2015). Thawing of the permafrost may lead to the disappearance or growth of thermokarst lakes (Smith et al., 2005), which may further affect greenhouse gas emissions and produce a feedback effect on climate change (Tarnocai et al., 2009; Schuur et al. 2009; Schaefer et al., 2011; McCalley et al., 2014). Additionally, changes in thermokarst lakes may both accelerate and delay permafrost thawing (Westermann et al., 2016; You et al., 2017).

5 Conclusions

This study evaluates the stability degradation of permafrost over the QTP from the 1960s to the 2000s based on the estimated decadal means of the mean annual air temperatures (MAATs) over the Qinghai-Tibet Plateau (QTP) in the past 50 years obtained by integrating remote sensing-based mean annual land surface temperatures (MASTs), leaf area index (LAI) and fractional snow cover values, and decadal mean MAATs measured at 152 weather stations using a geographically weighted regression (GWR) model. Cross validation shows that the accuracy of the estimated permafrost extent is greater than that of previous maps.

The decadal mean MAATs reflect a continuous rise at a rate of approximately 0.04 ℃/a during the past half century. The warming rate increases with increasing elevation from approximately 0.33 ℃ per decade at 3600 m to 0.49 ℃ per decade at 5200 m and then decreases as elevation increases further. Climate warming has led to the degradation of permafrost stability in the past half century. The area occupied by the stable permafrost types has continuously decreased, and the area occupied by the unstable permafrost types has continuously increased. The total degraded area is approximately 153.76×10^4 km^2, which accounts for 87.98% of the permafrost area in the 1960s. The stability for all permafrost types have degraded to lower levels. The extent of the extremely stable, stable, and sub-stable types retreated from the south to the north, whereas the extent of the transitional, unstable, and extremely unstable types extended northward. The mean elevations of the extremely stable, stable, sub-stable, transitional, unstable, and extremely unstable types increased by 88 m, 97 m, 155 m, 185 m, 161 m and 250 m, respectively. This result indicates that the climate sensitivity of permafrost is dependent on the stability level. The degradation mainly occurred during two periods that include the 1960s to the 1970s and the 1990s to the 2000s. The degradation of permafrost stability in the QTP has important impacts on the safety of infrastructure, flood risks, ecosystem resilience, and climate feedbacks, as well as the well-being of millions of people and sustainable development at the Third Pole.

The uncertainties inherent in this analysis cannot be discounted. These uncertainties are due to asynchronous changes in near-surface air temperatures and deep soil layer temperatures, the missing geothermal flux, insufficient resolution, or the inaccuracies and sparseness of the surface station data employed. As this evaluation is empirically based, obtaining more convincing results requires additional data, especially from the deep layers of soils. The development of new, fast, and inexpensive sensors and robust machine learning methods will assist in this effort. A physically based definition of permafrost stability and an improved physically based model will contribute to the prediction of permafrost stability degradation and its interactions with the engineering stability of infrastructure, the water cycle, and climate change.

Acknowledgements:

This study was jointly supported by the Chinese Academy of Sciences (CAS) Project Big Earth Data Engineering, two National Natural Science Foundation of China projects (41471359 and 91425303), and the Youth Innovation Promotion Association of the Chinese Academy of Sciences (grant number 2016375).

References

Brown, R. D. and Mote, P. W.: The response of Northern Hemisphere snow cover to a changing climate. Journal of Climate, 22(8), 2124-2145, 2009.

Brunsdon, C., Fotheringham, S., and Charlton, M.: Geographically weighted regression. Journal of the Royal Statistical Society: Series D (The Statistician), 47(3), 431-443, 1998.

Cheng, G. D.: Problems on zonation of high-altitude permafrost. ACTA Geographica Sinica, 39,185–193, 1984. (in Chinese)

Cheng, G.: Influences of local factors on permafrost occurrence and their implications for Qinghai-Xizang Railway design. Science in China Series D: Earth Sciences, 47(8), 704-709, 2004.

Cheng, G.: A roadbed cooling approach for the construction of Qinghai–Tibet Railway. Cold regions science and technology, 42(2), 169-176, 2005.

Cheng, G. D. and Wu, T. H.: Responses of permafrost to climate change and their environmental significance, Qinghai-Tibet Plateau. Journal of Geophysical Research, 112, F02S03, doi: 10.1029/2006JF000631, 2007.

Cheng, G., Sun, Z., and Niu, F.: Application of the roadbed cooling approach in Qinghai–Tibet railway engineering. Cold regions science and technology, 53(3), 241-258, 2008.

Cheng, W.M., Zhao, S.M., Zhou, C.H., and Chen, X.: Simulation of the Decadal Permafrost Distribution on the Qinghai-Tibet Plateau (China) over the Past 50 Years. Permafrost and Periglacial Processes, 23(4), 292–300, 2012.

Cheng, G.D. and Jin, H.J.: Permafrost and groundwater on the Qinghai-Tibet Plateau and in northeast China. Hydrogeology Journal, 21(1), 5–23, 2013.

Collett, T. S.: Energy resource potential of natural gas hydrates. AAPG bulletin, 86(11), 1971-1992, 2002.

Conrad, O., Bechtel, B., Bock, M., Dietrich, H., Fischer, E., Gerlitz, L., Wehberg, J., Wichmann, V., and Böhner, J.: System for automated geoscientific analyses (SAGA) v. 2.1. 4. Geoscientific Model Development, 8(7), 1991-2007, 2015.

Ding, Y. and Haeberli, W.: Compilation of long-term glacier-fluctuation data in China and a comparison with corresponding records from Switzerland. Journal of glaciology, 42(141), 389-400, 1996.

Garcia, D.: Robust smoothing of gridded data in one and higher dimensions with missing values. Computational Statistics & Data Analysis, 54, 1167-1178, 2010.

Giorgi, F., Hurrell, J. W., Marinucci, M. R., and Beniston, M.: Elevation dependency of the surface climate change signal: a model study. Journal of Climate, 10(2), 288-296, 1997.

Guo, W., Liu, S., Xu, J., Wu, L., Shangguan, D., Yao, X., Wei, J., Bao, W., Yu, P., Liu, Q., and Jiang, Z.: The second Chinese glacier inventory: data, methods and results. Journal of Glaciology, 61(226), 357-372, 2015.

Hachem, S., Allard, M., and Duguay, C.: Using the MODIS land surface temperature product for mapping permafrost: an application to Northern Quebec and Labrador, Canada. Permafrost and Periglacial Processes, 20(4), 407-416, 2009.

Hachem, S., Duguay, C. R., and Allard, M.: Comparison of MODIS-derived land surface temperatures with near-surface soil and air temperature measurements in continuous permafrost terrain. The Cryosphere, 6, 51-69, 2012.

Haeberli, W.: Investigating glacier – permafrost relationships in high-mountain areas: historical background, selected examples and research needs. In: Harris, C. and J.B. Murton (eds.): Cryospheric Systems – Glaciers and Permafrost. Geological Society Special Publication 242. London: 29–37, 2005.

Haeberli, W. and Hohmann, R.: Climate, glaciers and permafrost in the Swiss Alps 2050: scenarios, consequences and recommendations. In Proceedings Ninth International Conference on Permafrost, 1, 607-612, 2008.

Henderson-Sellers, A. and Hughes, N. A.: Albedo and its importance in climate theory. Progress in Physical Geography, 6(1), 1-44, 1982.

Hinzman, L. D., Deal, C. J., McGuire, A. D., Mernild, S. H., Polyakov, I. V., and Walsh, J. E.: Trajectory of the Arctic as an integrated system. Ecological Applications, 23(8), 1837-1868, 2013.

Huang, X., Deng, J., Wang, W., Feng, Q., and Liang, T. Impact of climate and elevation on snow cover using integrated remote sensing snow products in Tibetan Plateau. Remote Sensing of Environment, 190, 274-288, 2017.

International Permafrost Association (IPA).: IPA-IPY Thermal State of Permafrost (TSP) Snapshot Borehole Inventory, Version 1. Boulder, Colorado USA. NSIDC: National Snow and Ice Data Center. doi: 10.7265/N57D2S25, 2010.

Jin, H., Luo, D., Wang, S., Lü, L., and Wu, J.: Spatiotemporal variability of permafrost degradation on the Qinghai-Tibet Plateau. Sciences in Cold and Arid Regions, 3(4), 281-305, 2011.

Jin, H., Zhao, L., Wang, S., and Jin, R.: Thermal regimes and degradation modes of permafrost along the Qinghai-Tibet Highway. Science in China Series D: Earth Sciences, 49(11), 1170-1183, 2006.

Jorgenson, M. T., Romanovsky, V., Harden, J., Shur, Y., O'Donnell, J., Schuur, E. A., Kanevskiy, M., and Marchenko, S.: Resilience and vulnerability of permafrost to climate change. Canadian Journal of Forest Research, 40(7), 1219-1236, 2010.

Kogan, F., Powell, A., and Fedorov, O.: Use of Satellite and In-Situ Data to Improve Sustainability. Springer, 2011.

Kumar, S., Lal, R., and Liu, D.: A geographically weighted regression kriging approach for mapping soil organic carbon stock. Geoderma, 189, 627-634, 2012.

Lawrence, D. M., Slater, A. G., Romanovsky, V. E., and Nicolsky, D. J.: Sensitivity of a model projection of near-surface permafrost degradation to soil column depth and representation of soil organic matter. Journal of Geophysical Research: Earth Surface, 113(F2), 2008.

Lawrence, D. M., Oleson, K. W., Flanner, M. G., Thornton, P. E., Swenson, S. C., Lawrence, P. J., Zeng X.B., Yang Z. L., Levis, S., Sakaguchi, K., Bonan, G. B., and Slater, A. G.: Parameterization improvements and functional and structural advances in version 4 of the Community Land Model. Journal of Advances in Modeling Earth Systems, 3(1), 2011.

Larsen, P. H., Goldsmith, S., Smith, O., Wilson, M. L., Strzepek, K., Chinowsky, P., and Saylor, B.: Estimating future costs for Alaska public infrastructure at risk from climate change. Global Environmental Change,18(3), 442-457, 2008.

Li, X., Cheng, G., Jin, H., Kang, E., Che, T., Jin, R., Wu, L., Nan, Z.T., Wang, J., and Shen, Y.: Cryospheric change in China. Global and Planetary Change, 62(3), 210-218, 2008.

Li, S. D. and Cheng, G.D.: Map of permafrost on the Qinghai-Tibet Plateau (1:3,000,000). Gansu Culture Press: Lanzhou, 1996. (in Chinese).

Li, S., Cheng, G., and Guo, D.: The future thermal regime of numerical simulating permafrost on Qinghai-Xizang (Tibet) Plateau, China, under climate warming. Science in China Series D-earth Sciences, 39(4), 434-441, 1996.

Lin, Z., Niu, F., Xu, Z., Xu, J., and Wang, P.: Thermal regime of a thermokarst lake and its influence on permafrost, Beiluhe Basin, Qinghai-Tibet Plateau. Permafrost and Periglacial Processes, 21(4), 315-324, 2010.

Liu, X. and Chen, B.: Climatic warming in the Tibetan Plateau during recent decades. International journal of climatology, 20(14), 1729-1742, 2000.

Liu, X. D., Yin, Z.Y., Shao, X. M., and Qin, N. S.: Temporal trends and variability of daily maximum and minimum, extreme temperature events, and growing season length over the eastern and central Tibetan Plateau during 1961–2003. Journal of Geophysical Research, 111(D19109), doi:10.1029/2005JD006915, 2006.

Liu, X., Cheng, Z., Yan, L., and Yin, Z. Y.: Elevation dependency of recent and future minimum surface air temperature trends in the Tibetan Plateau and its surroundings. Global and Planetary Change, 68(3), 164-174, 2009.

Luo, D. L., Jin, H. J., Lin, L., You, Y. H., Yang, S. Z., and Wang, Y. P.: Distributive features and controlling factors of permafrost and the active layer thickness in the Bayan Har Mountains along the Qinghai-Kangding Highway on Northeastern Qinghai-Tibet Plateau. Scient Geograph Sin, 33, 635-640, 2013. (In Chinese, English abstract)

Luo, J., Niu, F., Lin, Z., Liu, M., and Yin, G.: Thermokarst lake changes between 1969 and 2010 in the beilu river basin, qinghai–tibet plateau, China.Science Bulletin, 60(5), 556-564, 2015.

McCalley, C. K., Woodcroft, B. J., Hodgkins, S. B., Wehr, R. A., Kim, E. H., Mondav, R., Crill, P.M., Chanton, J. P., Rich, V.I., Tyson, G.W., and Saleska, S. R.: Methane dynamics regulated by microbial community response to permafrost thaw. Nature, 514(7523), 478-481, 2014.

Mu, C., Zhang, T., Wu, Q., Peng, X., Cao, B., Zhang, X., and Cheng, G.: Editorial: Organic carbon pools in permafrost regions on the Qinghai–Xizang (Tibetan) Plateau. The Cryosphere, 9(2), 479-486, 2015.

Nan, Z. T., Li, S. X., and Liu, Y, Z.: Mean annual ground temperature distribution on the Tibetan Plateau: Permafrost distribution mapping and further application. Journal of Glaciology and Geocryology, 24(2), 142-148, 2002. (in Chinese)

Nan, Z., Gao, Z., Li, S., and Wu, T.: Permafrost changes in the northern limit of permafrost on the Qinghai-Tibet Plateau in the last 30 years. Acta Geographica Sinica, 58(6): 817–823, 2003. (In Chinese, English abstract)

Niu, F., Lin, Z., Liu, H., and Lu, J.: Characteristics of thermokarst lakes and their influence on permafrost in Qinghai–Tibet Plateau. Geomorphology,132(3), 222-233, 2011.

Otto, J. C., and Keuschnig, M.: Permafrost-Glacier Interaction–Process Understanding of Permafrost Reformation and Degradation. permAfrost–Austrian Permafrost Research Initiative. Final Report, Innsbruck: Institute for Interdisciplinary Mountain Research, ÖAW, 3-16, 2014.

Permafrost Subcommittee, National Research Council of Canada.: Glossary of Permafrost and Related Ground-ice Terms. National Research Council of Canada Technical Memorandum, 1988.

Pepin, N., Bradley, R. S., Diaz, H. F., Baraer, M., Caceres, E. B., Forsythe, N., Fowler, H., Greenwood, G., Hashmi, M. Z., Liu, X. D., Miller, J. R., Ning, L., Ohmura, A., Palazzi, E., Rangwala, I., Schöner, W., Severskiy, I., Shahgedanova, M., Wang, M. B., Williamson, S. N., and Yang, D. Q.: Elevation-dependent warming in mountain regions of the world. Nature Climate Change, 5, 424-430, 2015.

Qin, J., Yang, K., Liang, S., and Guo, X.: The altitudinal dependence of recent rapid warming over the Tibetan Plateau. Climatic Change, 97, 321-327, 2009.

Ran, Y., Li, X., Cheng, G., Zhang, T., Wu, Q., Jin, H., and Jin, R.: Distribution of permafrost in China: an overview of existing permafrost maps. Permafrost and Periglacial Processes, 23(4), 322-333, 2012.

Ran, Y., Li, X., Jin, R., and Guo, J.: Remote sensing of the mean annual surface temperature and surface frost number for mapping permafrost in China. Arctic, Antarctic, and Alpine Research, 47(2), 255-265, 2015.

Ran, Y. H. and Li, X.: Evaluation of the permafrost stability degradation from 1980 to 2010 in China. Sciences in Cold and Arid Regions, 8(5), 0359–0366, doi: 10.3724/SP.J.1226.2016.00359, 2016.

Ran, Y.H., Li, X., and Cheng, G.D.: A permafrost thermal stability map over third pole by integrated remotely sensed land surface temperature, leaf area index, soil properties, and ground boreholes measurement. Submitted to Remote Sensing of Environment, 2017.

Schaefer, K., Zhang, T., Bruhwiler, L., and Barrett, A. P.: Amount and timing of permafrost carbon release in response to climate warming. Tellus B, 63(2), 165-180, 2011.

Schuur, E. A., Vogel, J. G., Crummer, K. G., Lee, H., Sickman, J. O., and Osterkamp, T. E.: The effect of permafrost thaw on old carbon release and net carbon exchange from tundra. Nature, 459(7246), 556-559, 2009.

Smith, M. W. and Riseborough, D. W.: Permafrost monitoring and detection of climate change. Permafrost and Periglacial Processes, 7(4), 301-309, 1996.

Smith, M. W., and Riseborough, D. W.: Climate and the limits of permafrost: a zonal analysis. Permafrost Periglacial Process, 13, 1-15, 2002.

Smith, L. C., Sheng, Y., MacDonald, G. M., and Hinzman, L. D. Disappearing arctic lakes. Science, 308(5727), 1429-1429, 2005.

Sun, Z. Z., Wu, G. L., Yun, H. B., Liu, G. J., and Rui, P. F.: Permafrost degradation under an embankment of the Qinghai-Tibet Railway in the southern limit of permafrost. Journal of Glaciology and Geocryology, 36(4), 767-771, doi: 10.7522/j.issn.1000-0240.2014.0092, 2014. (In Chinese, English abstract)

Stehman, S. V.: Selecting and interpreting measures of thematic classification accuracy. Remote sensing of Environment, 62(1), 77-89, 1997.

Stieglitz, M., Déry, S. J., Romanovsky, V. E., and Osterkamp, T. E.: The role of snow cover in the warming of arctic permafrost. Geophysical Research Letters, 30(13), 2003.

Tang, Z., Wang, J., Li, H., and Yan, L.: Spatiotemporal changes of snow cover over the Tibetan plateau based on cloud-removed moderate resolution imaging spectroradiometer fractional snow cover product from 2001 to 2011. Journal of Applied Remote Sensing, 7(1), 073582-073582, 2013.

Tarnocai, C., Canadell, J. G., Schuur, E. A. G., Kuhry, P., Mazhitova, G., and Zimov, S.: Soil organic carbon pools in the northern circumpolar permafrost region. Global biogeochemical cycles, 23(2), 2009.

Vancutsem, C., Ceccato, P., Dinku, T., & Connor, S. J.: Evaluation of MODIS land surface temperature data to estimate air temperature in different ecosystems over Africa. Remote Sensing of Environment, 114(2), 449-465, 2010.

Wan, Z., Zhang, Y., Zhang, Q., and Li, Z.L.: Validation of the land-surface temperature products retrieved from Terra Mode rate Resolution Imaging Spectroradiometer data. Remote Sensing of Environment, 83, 163-180, 2002.

Wan, Z., Zhang, Y., Zhang, Q., and Li, Z.L.: Quality assessment and validation of the MODIS global land surface temperature. International Journal of Remote Sensing, 25, 261-274, 2004.

Wan, Z.: New refinements and validation of the MODIS land-surface temperature/emissivity products. Remote Sensing of Environment, 112(1): 59-74, 2008.

Wang, S.L., Jin, H.J., Li, S.X., and Zhao, L.: Permafrost degradation on the Qinghai-Xizang (Tibet) Plateau and its environmental impacts. Permafrost and Periglacial Processes, 11, 43–53, 2000.

Wang, G., Garcia, D., Liu, Y., de Jeu, R., and Dolman, A.J.: A three dimensional gap filling method for large geophysical datasets: application to global satellite soil moisture observations. Environmental Modelling & Software, 30, 139-142, 2012.

Wang, Q. F., Zhang, T. J., Wu, J. C., Peng, X. Q., Zhong, X. Y., Mou, C., Wang, K., Wu, Q. B., and Cheng, G. D.: Investigation on permafrost distribution over the upper reaches of the Heihe River in the Qilian Mountains. Journal of Glaciology and Geocryology, 35(1), 19-25, 2013. (In Chinese, English abstract)

Wang, T., Peng, S., Lin, X., and Chang, J.: Declining snow cover may affect spring phenological trend on the Tibetan Plateau.Proceedings of the National Academy of Sciences, 110(31), E2854-E2855, 2013.

Wang, W., Feng, Q., Yu, H., Liang, T., and Guo, N.: Spatio-temporal change of vegetation on Tibetan Plateau based on AVHRR-NDVI data. In Geoscience and Remote Sensing Symposium (IGARSS), 2016 IEEE International (pp. 1374-1377). IEEE.

Westermann, S., Langer, M., Boike, J., Heikenfeld, M., Peter, M., Etzelmüller, B., and Krinner, G. Simulating the thermal regime and thaw processes of ice-rich permafrost ground with the land-surface model CryoGrid 3. Geoscientific Model Development, 9, 523-546, 2016.

Williams, P. J. and Smith, M.W.: The frozen earth: fundamentals of geocryology. UK, Cambridge: Cambridge University Press, 1989.

Wu, Q.B., Zhu, Y.L., and Liu, Y.Z.: Evaluation model of permafrost thermal stability and thawing sensibility under engineering activity. Cold Regions Science and Technology, 34(1), 19–30, 2002.

Wu, J., Sheng, Y., Wu, Q., and Wen, Z.: Processes and modes of permafrost degradation on the Qinghai-Tibet Plateau. Science China Earth Sciences, 53(1), 150-158, 2010a.

Wu, Q. B., Zhang, Z. Q., and Liu, Y. Z.: Long-term thermal effect of asphalt pavement on permafrost under embankment. Cold Regions Science and Technology, 60: 221–229, 2010b.

Wu, D., Zhao, X., Liang, S., Zhou, T., Huang, K., Tang, B., and Zhao, W.: Time-lag effects of global vegetation responses to climate change. Global change biology, 21(9), 3520-3531, 2015.Xiang, Y., Xiao, Z. Q., Ling, S. L., Wang, J. D., and Song, J. L.: Validation of Global LAnd Surface Satellite (GLASS) leaf area index product. J. Remote Sens, 18, 573-596, 2014.

Xiao, Z., Liang, S., Wang, J., Chen, P., Yin, X., Zhang, L., and Song, J.: Use of general regression neural networks for generating the GLASS leaf area index product from time-series MODIS surface reflectance. IEEE Transactions on Geoscience and Remote Sensing, 52(1), 209-223, 2014.

Yang, M., Nelson, F. E., Shiklomanov, N. I., Guo, D., and Wan, G.: Permafrost degradation and its environmental effects on the Tibetan Plateau: A review of recent research. Earth-Science Reviews, 103(1), 31-44, 2010.

Yao, Y. and Zhang, B.: MODIS-based estimation of air temperature of the Tibetan Plateau. Journal of Geographical Sciences, 23(4), 627-640, 2013.

Ye, B. S., Ding, Y. J., and Liu, C. H.: Response of Valley Glaciers in Various Size and Their Runoff to Climate Change. Journal of Glaciolgy and Geocryology, 23(2), 103-110, 2001. (In Chinese, English abstract)

Yoshikawa, K., and Hinzman, L. D.: Shrinking thermokarst ponds and groundwater dynamics in discontinuous permafrost near Council, Alaska. Permafrost and Periglacial Processes, 14(2), 151-160, 2003.

You, Y., Yu, Q., Pan, X., Wang, X., Guo, L., and Wu, Q. Thermal effects of lateral supra-permafrost water flow around a thermokarst lake on the Qinghai-Tibet Plateau. Hydrological Processes, 1-9, 2017.

Yuan, X., Wang, W., Cui, J., Meng, F., Kurban, A., and De Maeyer, P.: Vegetation changes and land surface feedbacks drive shifts in local temperatures over Central Asia. Scientific Reports,7, 2017.

Yu, H., Wu, Q. B., and Liu, Y. Z.: The long-term monitoring system on permafrost regions along the Qinghai-Tibet Railway. Journal of Glaciology and Geocryology, 30(3), 475-481, 2008. (In Chinese, English abstract)

Zhang, T.: Influence of the seasonal snow cover on the ground thermal regime: An overview. Reviews of Geophysics, 43(4), 2005.

Zhang, G., Yao, T., Xie, H., Kang, S., and Lei, Y.: Increased mass over the Tibetan Plateau: from lakes or glaciers?. Geophysical Research Letters, 40(10), 2125-2130, 2013.

Zhao, L., Wu, Q., Marchenko, S. S., and Sharkhuu, N.: Thermal state of permafrost and active layer in Central Asia during the International Polar Year. Permafrost and Periglacial Processes, 21(2), 198-207, 2010.

Zhong, L., Ma, Y., Salama, M. S., and Su, Z.: Assessment of vegetation dynamics and their response to variations in precipitation and temperature in the Tibetan Plateau. Climatic Change, 103(3-4), 519-535, 2010.

Zhu, Z., Kang, G., Ma, Y., Xie, Q., Zhang, D., and Ning, J.: Temperature damage and constitutive model of frozen soil under dynamic loading. Mechanics of Materials, 102, 108-116, 2016.

Zou, D., Zhao, L., Sheng, Y., Chen, J., Hu, G., Wu, T., Wu, J., Xie, C., Wu, X., Pang, Q., Wang, W., Du, E., Li, W., Liu, G., Li J., Qiu, Y., Qiao, Y., Wang, W., Shi, J., and Cheng, G.: A New Map of the Permafrost Distribution on the Tibetan Plateau. The Cryosphere Discuss., doi:10.5194/tc-2016-187, 2016.

Table 1. Classification system used to assess permafrost stability (Cheng, 1984)

Type	Mean annual ground temperature (℃)	Thickness of permafrost (m)	Mean annual air temperature (℃)
Extremely stable	<-5.0	170	<-8.5
Stable	-3.0~-5.0	110~170	-6.5~-8.5
Sub-stable	-1.5~-3.0	60~110	-5.0~-6.5
Transitional	-0.5~-1.5	30~60	-4.0~-5.0
Unstable	+0.5~-0.5	0~30	-2.0~-4.0
Extremely unstable	>+0.5		-1.0~-2.0

Table 2. The statistics of the stepwise linear regression analysis

Model	Independent variables	Adjusted R^2
1	MAST	0.83
2	MAST, LAI	0.87
3	MAST, LAI, FSC	0.88
4	MAST, LAI, FSC, Elevation	0.90
5	MAST, LAI, FSC, Elevation, Longitude	0.91
6	MAST, LAI, FSC, Elevation, Longitude, Latitude	0.93

Table 3. The area statistics of the permafrost thermal stability types over the QTP in the past 50 years ($\times 10^4$ km^2)

Permafrost stability	1960s	1970s	1980s	1990s	2000s	Net change (1960s to 2000s)		2000s excluding glaciers	Change rate ($\times 10^4$ km^2/decade)
						Area	Percent (%)		
remely stable	12.35	8.56	8.74	5.66	3.36	-8.99	-72.79	1.86	-2.09
Stable	38.59	28.30	27.64	20.91	11.53	-27.06	-70.12	10.39	-6.15
Sub-stable	34.14	34.75	34.09	31.94	24.84	-9.30	-27.24	24.03	-2.14
Transitional	24.73	23.95	23.59	23.39	23.55	-1.18	-4.77	23.12	-0.29
Unstable	44.22	43.89	43.70	46.51	48.21	3.99	9.02	47.80	1.06
Extremely unstable	20.73	21.05	20.54	20.16	21.63	0.90	4.34	21.56	0.09
Total area	174.76	160.50	158.32	148.57	133.10	-41.66	-23.84	128.76	-9.52

Table 4. Transfer matrix of permafrost stability types from the 1960s to the 2000s in the QTP (%)

2000s \ 1960s	Extremely stable	Stable	Sub-stable	Transitional	Unstable	Extremely unstable	Seasonally frozen ground
Extremely stable	24.75	0.78	0.00	0.00	0.00	0.00	0.00
Stable	59.42	9.67	1.33	0.02	0.00	0.00	0.00
Sub-stable	15.82	50.93	8.37	1.45	0.03	0.00	0.00
Transitional	0.00	35.91	23.18	6.16	0.57	0.00	0.00
Unstable	0.00	2.72	67.07	66.82	17.19	0.66	0.00
Extremely unstable	0.00	0.00	0.05	25.49	32.80	3.39	0.12
Seasonally frozen ground	0.00	0.00	0.00	0.06	49.40	95.95	99.88
Class changes	75.25	90.34	91.63	93.84	82.81	96.61	0.13

Table 5. The mean change in elevation of the permafrost thermal stability types over the QTP in the past 50 years (unit: metre)

Permafrost stability	1960s	1970s	1980s	1990s	2000s	Rate (m/decade)	R^2
Extremely stable	5240	5161	5169	5232	5328	24.7	0.34
Stable	5050	5052	5055	5094	5147	23.6	0.80
Sub-stable	4881	4932	4937	4985	5036	36.3	0.96
Transitional	4756	4799	4804	4859	4941	43.0	0.91
Unstable	4614	4670	4675	4713	4775	36.5	0.94
Extremely unstable	4392	4503	4513	4565	4642	56.2	0.94

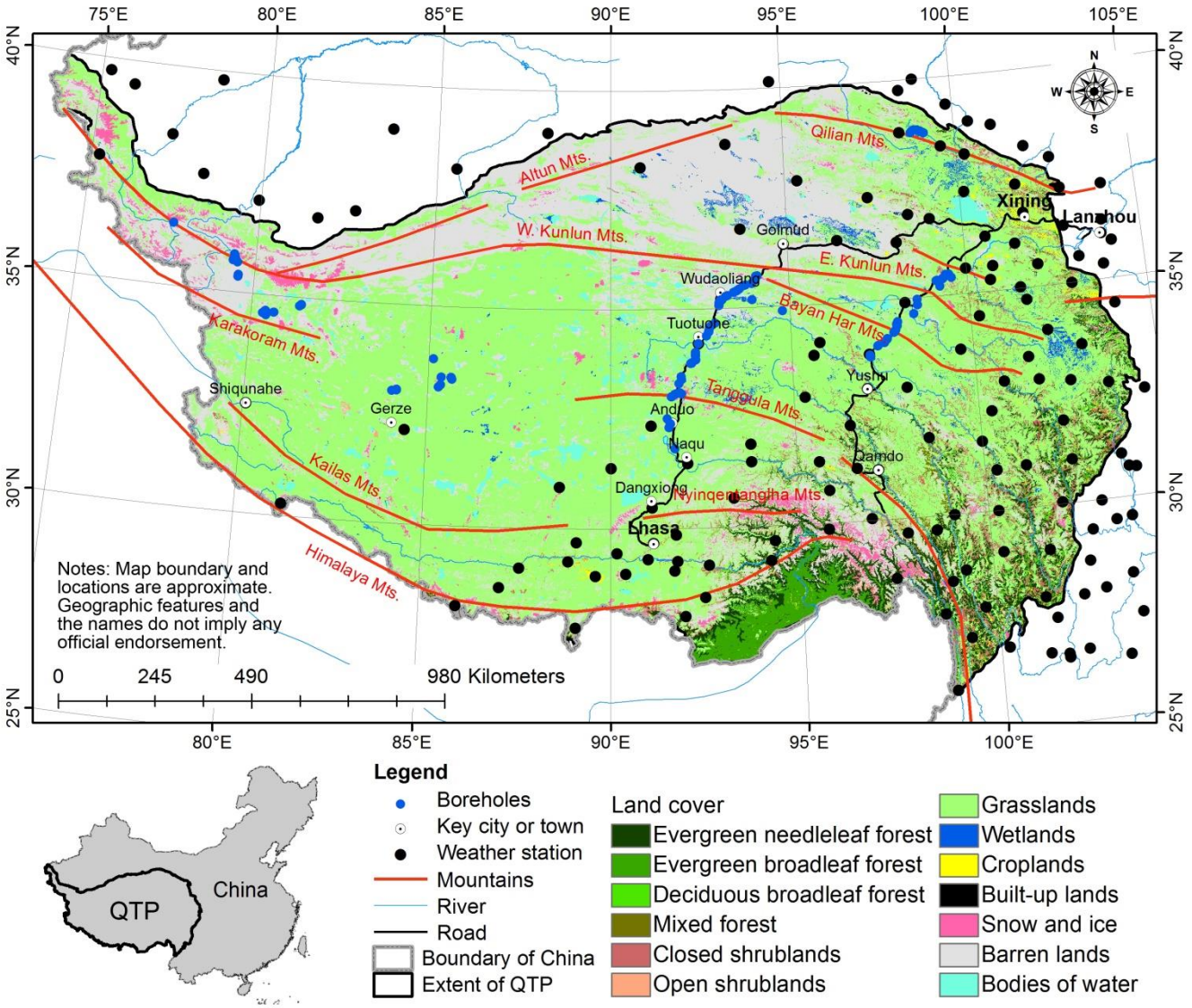

Figure 1. The distribution of in situ MAAT observation stations and MAGT boreholes over the QTP.

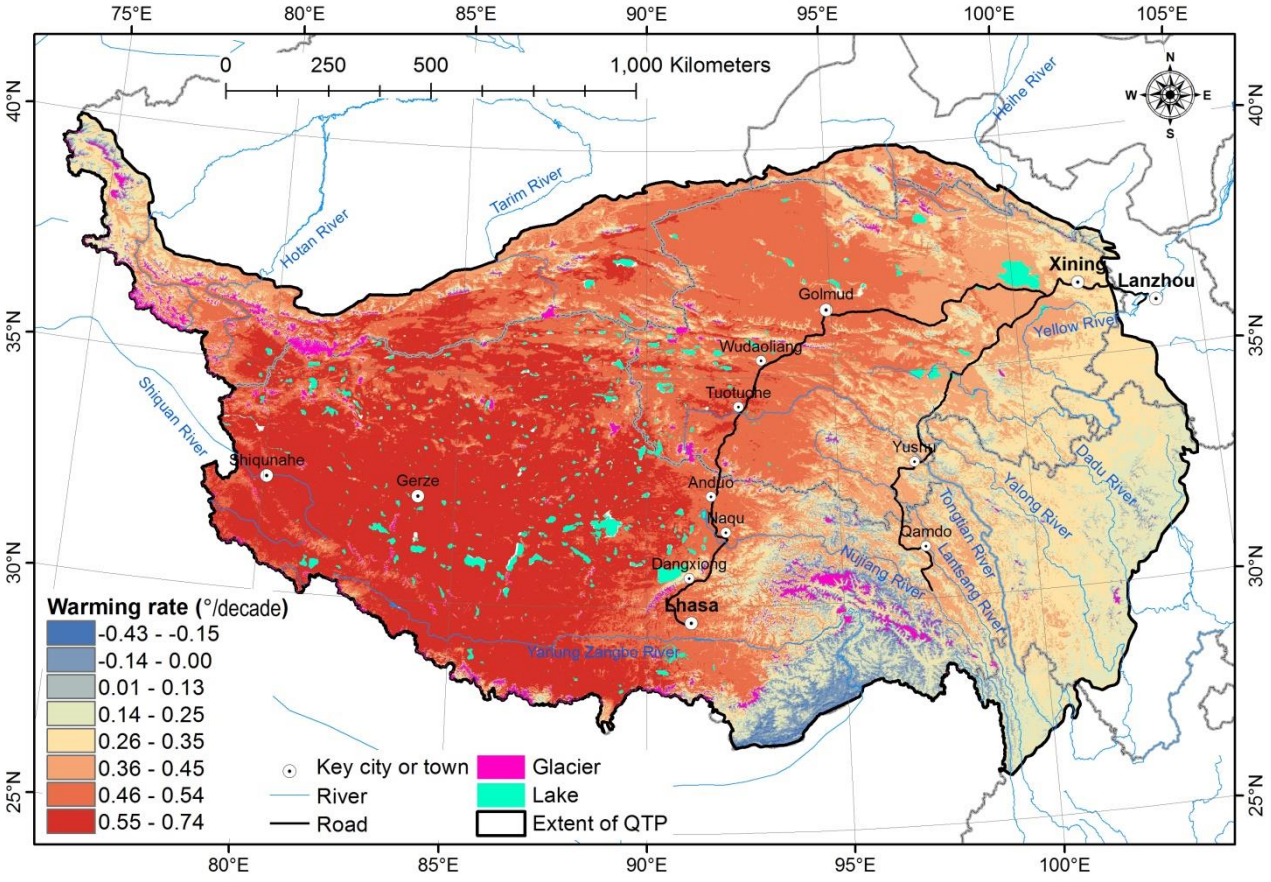

Figure 2. Spatial variability of MAAT warming rates over the QTP in the past 50 years.

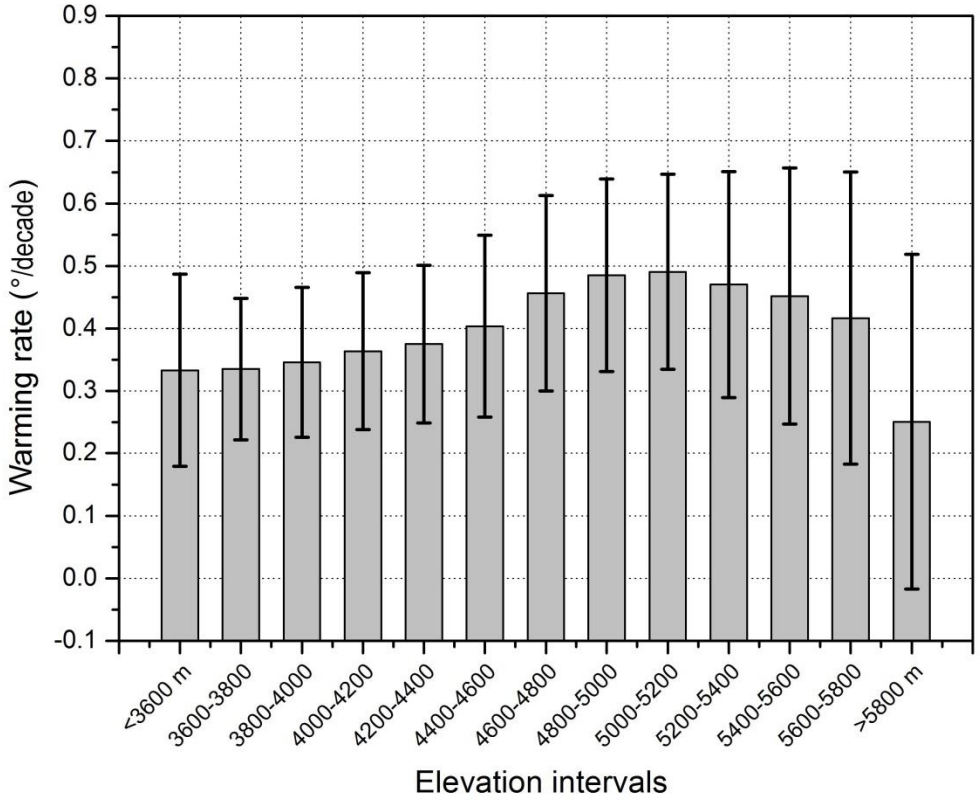

Figure 3. Warming rates with increasing elevation. These rates are derived from MAATs estimated using MODIS LSTs. Error bars display the standard deviations.

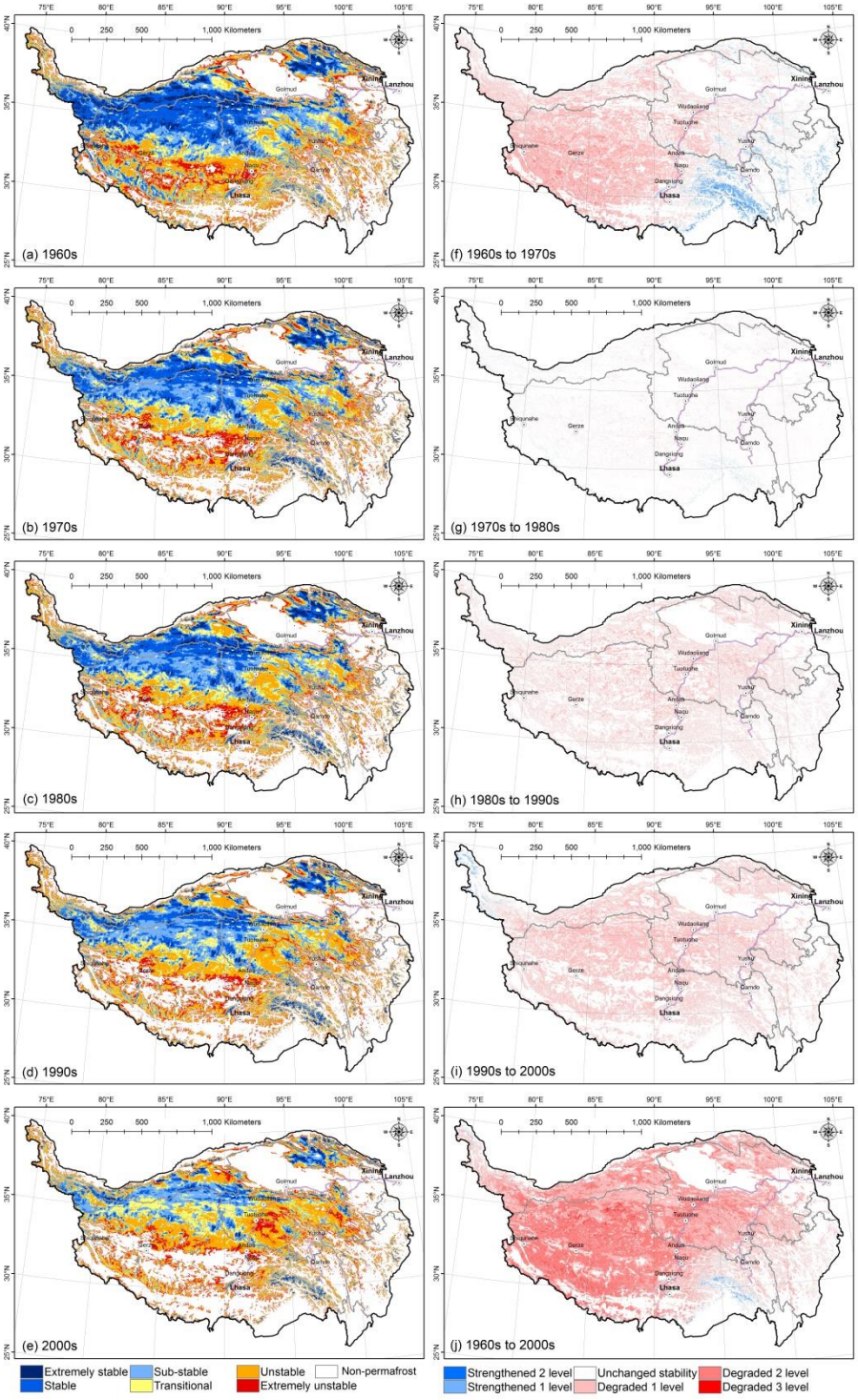

Figure 4. The permafrost stability map in each decade (a-e) and its spatial changes from the 1960s to the 2000s (f-j) over the QTP during the past 50 years.

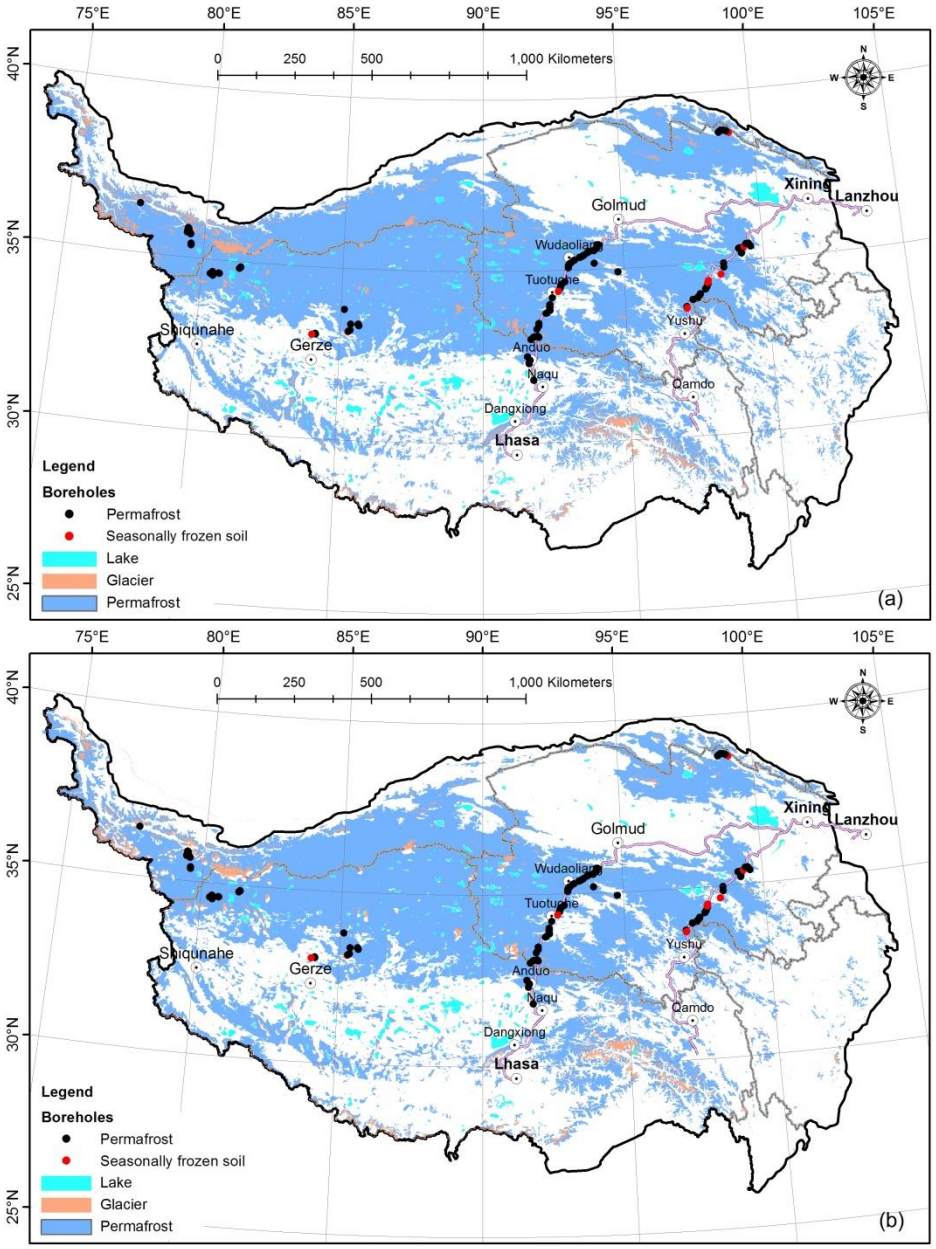

Figure 5. Comparison of the permafrost extent between the results of this study (a) and the permafrost map presented by Zou et al., (2016) (b).